Combined nonlinear wave and current induced instantaneously-liquefied soil depth in a non-cohesive seabed

Li-Jing Yang [a,b], Fu-Ping Gao [a,b,*], Chang-fei Li [a,b]

[a] *Institute of Mechanics, Chinese Academy of Sciences, Beijing, 100190, China*
[b] *School of Engineering Science, University of Chinese Academy of Sciences, Beijing, 100049, China*

ARTICLE INFO

ABSTRACT

Progressive waves usually coexist with a steady current in coastal environments. Superposing a following or opposite current onto the progressive waves could significantly alter the excess pore-water pressure distribution within the seabed. Unlike previous studies which were predominantly limited to the pure wave cases, the instantaneous liquefaction of a non-cohesive seabed is investigated analytically under the combined loading of 3rd order Stokes waves and a steady current. Explicit expressions are derived for the transient pore pressure distribution in a seabed with instantaneously-liquefied zone and the corresponding instantaneous liquefaction depth, which are verified by degradation analyses and comparisons with the existing offshore field observations. The phase lag of excess pore pressure is taken into account in the theoretical derivation. Parametric study is then performed to examine the effects of wave non-linearity and superimposing a current on the instantaneous liquefaction depth. It is indicated that wave-nonlinearity effects on the instantaneous liquefaction depth are not neglectable, especially when the wave height gets larger and the current velocity is reduced. The envelope for the variation of maximum instantaneous liquefaction depth with both wave period and current velocity is further constructed. To superimpose an opposing current onto the progressive waves with a relatively small wave period could be beneficial for the prevention of instantaneous liquefaction. Nevertheless, the variation trends of the maximum instantaneous liquefaction depth are attributed to the synthetical effect of the alternations of both wavelength and wave height during nonlinear wave-current interactions.

1. Introduction

While ocean waves are propagating over a porous seabed, periodic pore pressure may be generated within the soil, which could further cause seabed liquefaction. In the past few decades, catastrophic consequences to marine structures due to seabed liquefaction have been reported frequently, e.g., Christian et al. (1974); Miyamoto et al. (1989); Sumer et al. (1999); De Groot et al. (2006). Both residual and transient mechanisms for the pore pressures under the action of progressive waves have been observed in the wave flumes and offshore fields (see Zen and Yamazaki, 1991; Sassa et al., 2006; Jeng et al., 2007). To some extent, wave-induced residual liquefaction of the seabed is similar to the soil liquefaction during earthquake events (see the pioneering work by Seed and Lee, 1966), where the effective stress was reduced to nil due to the pore pressure buildup (see the review on soil liquefaction modeling by Sawicki and Mierczyński, 2006). In contrast to the residual liquefaction that takes place in a non-cohesive seabed (Sassa and Sekiguchi, 1999,

2001; Sumer, 2014), instantaneous liquefaction (also referred as "momentary liquefaction") is essentially caused by the instantaneous upward seepage within the upper layer of the seabed under wave troughs (see Qi and Gao, 2018).

Based on Biot's poroelastic theory (Biot, 1941), wave-induced transient pore pressure responses have been investigated analytically under various seabed conditions (see Sumer, 2014; Jeng, 2018): e.g., the infinite thickness of the seabed by Yamamoto et al. (1978); the arbitrary thickness of a horizontally layered seabed by Madsen (1978); and the finite thickness of the seabed by Hsu and Jeng (1994). A boundary-layer approximation was developed by Mei and Foda (1981) for wave-induced stress in a porous elastic medium. In addition to analytical investigations, numerical and physical models were also employed to investigate the pore pressure responses in the seabed under complex structure boundaries and wave loading conditions, e.g., the wave-breakwater-seabed interaction (Mase et al., 1994; Vanneste and Troch, 2012; Jensen et al., 2014), the wave-monopile-seabed interaction

---

(Li et al., 2011; Lin et al., 2017; Zhao et al., 2017; Duan et al., 2019; Miyamoto et al., 2021), the wave-pipeline-seabed interaction (Gao et al., 2003; Miyamoto et al., 2019; Qi et al., 2020; Shi et al., 2021), and the breaking wave-seabed interaction (Li et al., 2021). Recently, a numerical toolbox was established by Li et al. (2020) for wave-induced seabed response analysis around marine structures in the OpenFOAM® framework.

In a fully saturated sandy seabed, instantaneous liquefaction is hardly to occur due to the extremely slow attenuation of pore pressure downward deeply into the seabed. Nevertheless, it is not uncommon for gas to be found in submarine sediments (Okusa, 1985). The presence of methane, common in the Mississippi Delta sediments, has been reported to influence the wave-induced pore pressures (see Okusa, 1985). The biogenic degradation of organic matters can release gas within the subsea sediments (Judd and Hovland, 2007). In the nearshore, especially at the surf zones, the air can be introduced into the seabed at ebb tides and partially trapped in the porous soil with rising tides (Mory et al., 2007). Using a geo-endoscopic camera, Michallet et al. (2009) measured the gas content within the sand bed on the Atlantic coast of Aquitaine, in southwest France. They found that the gas content was up to 6.0% (i.e., saturation degree = 94.0%) at the soil depth of 0.25 m below the seabed surface. In such an unsaturated seabed at shallow waters, pore pressure attenuation could be significant, leading to an instantaneous liquefaction risk.

Several criteria have been proposed to predict the instantaneous liquefaction of the seabed under wave loading. The criterion firstly proposed by Bear (1972) (denoted as "criterion-I″") was from the perspective of soil-element (or termed micro-layer) scale. For the criterion-I, the vertical gradient of excess pore pressure (j_z) inducing the upward seepage force within the seabed under wave troughs must locally overcome the buoyant unit weight of soil (γ'), i.e., $j_z - \gamma' \geq 0$. Zen and Yamazaki (1990) later deduced a criterion for instantaneous liquefaction (denoted as "criterion-II") from the traditional force analysis on the vertical soil-column rather than the soil-element analysis in criterion-I. The criterion-II suggested that instantaneous liquefaction could occur if the excess pore pressure difference between a certain depth ($p(z)$) and the soil surface (P_b) becomes larger than the overburden soil pressure (σ'_{z0}), i.e., $p(z) - P_b \geq \sigma'_{z0}$. Considering the cohesion and the internal friction angle of soil, Ye (2012) proposed three-dimensional (3D) liquefaction criteria and further made a discussion on the existing criteria, e.g., the criterion-II, and the criterion by Jeng (1997); and the 1D criterion by Zen and Yamazaki (1990) (i.e., criterion-II) was recommended to use in engineering. As aforementioned, instantaneous liquefaction is induced by the upward seepage under wave troughs; and in the fields, the observed instantaneously-liquefied depth (<3 m or less; see Zen and Yamazaki (1991)) is generally much smaller than the wavelength ($\sim 10^2$ m). As such, the instantaneous liquefaction can be essentially regarded as a quasi-1D process.

Nevertheless, if such criteria in the inequality forms (e.g., criterion-I and –II) are adopted for a non-cohesive seabed, an upward resultant force could be unreasonably generated in the instantaneously-liquefied soil and the upper layer of soil mass would be sucked away, which is fallacious in physics. To avoid such a fallacy, Qi and Gao (2018) proposed an improved criterion for instantaneous liquefaction of a non-cohesive seabed (denoted as "criterion-III"). The criterion-III implied that the vertical gradient of excess pore pressure (j_z) should be identical to the buoyant unit weight of the soil (γ') in an instantaneously-liquefied soil layer, i.e., $j_z - \gamma' \equiv 0$, which was verified with offshore field observations by Mory et al. (2007) and the multi-scale numerical simulations by Scholtès et al. (2015). Based on the criterion-III, an analytical solution for instantaneous liquefaction depth was further derived by Qi and Gao (2018). To efficiently avoid resulting in fallacious tensile stresses in a non-cohesive seabed in previous numerical simulations, Zhou et al. (2020, 2021) recently proposed a

non-Darcy flow model for the instantaneously-liquefied seabed by taking account of the criterion-III and the Karush–Kuhn–Tucker condition. Note that, in the previous investigations, the seabed liquefaction under pure waves was mainly involved, but the combined wave-current effects have not been intensively investigated.

In coastal environments, the coexistence of periodic waves and a steady current is more frequently encountered than pure waves. It is mainly near continental margins and in shallow seas that currents influence waves significantly (see Peregrine, 1976). With the increasing number of subsea structures (e.g., for the rapid development of nearshore windfarms), the prediction of seabed liquefaction under the combined wave-current loading is of growing importance. As for the wave-current interactions, Longuet-Higgins and Stewart (1960, 1961) introduced a term called radiation stress in the governing equation to well describe the wave-current energy exchange. Whitham (1962) further established the governing equations for the conservations of mass, momentum, and energy regarding wave-current interactions. Later, the characteristic parameters for waves and current due to the interactions between waves and a uniform current were investigated experimentally & numerically (e.g., Thomas, 1981; Baddour and Song, 1990) and analytically (Zou, 2004). To describe the water particle movements in a non-linear wave-current interaction flow, Hsu et al. (2009) derived a third-order trajectory solution in the Lagrangian form based on a Euler-Lagrange transformation. From the trajectories of water particles resulting from wave-current interactions, it was found that particle displacement near the surface decreases due to its mass transport velocity resisted by an opposing current. The analytical solution by Hsu et al. (2009) provided an accurate prediction for the free surface elevations for large Froude numbers associated with a uniform current.

Under the combined wave-current loading, the spatio-temporal distribution of excess pore pressures could be altered from those for pure waves, as observed in the large wave-current flume (Qi et al., 2012, 2019). Based on the u-p approximation for Biot's poroelastic dynamic theory (Biot, 1956), Ye and Jeng (2012) numerically investigated the pore pressure responses of a sandy seabed under combined nonlinear waves and a uniform current. Analytical approximation for combined wave-current induced pore pressure responses in an un-liquefied seabed was later derived by Zhang et al. (2013). It has been recognized that wave-induced transient pore pressure within the seabed could be significantly affected by superimposing a following or opposite current. It should be noted that the wave height was assumed unchanged after the current is superimposed onto the progressive waves in the numerical simulation (Ye and Jeng, 2012) and the analytical derivation (Zhang et al., 2013). Flume observation by Qi et al. (2019) showed that the wave height was reduced and the corresponding wavelength was elongated with increasing the velocity of a following current. A similar trend regarding the influence of current on both wave height and wavelength was ever obtained for analyzing the residual liquefaction of the seabed under combined wave-current loading (Sumer, 2014). Such variations of wave height and wavelength during wave-current interactions could also affect the instantaneous liquefaction. Accurate prediction of the instantaneously-liquefied depth is vital for subsea foundations, especially in the coastal zones where the waves and current are usually coexisting. Once the liquefaction occurs, the soil particles will become suspended with the pore pressure response adjusted (Zen and Yamazaki, 1991; Mory et al., 2007). Nevertheless, the effect of liquefaction was not considered in the previous analytical study on the pore pressure induced by combined wave-current loading (Zhang et al., 2013), and the existing analytical solutions for instantaneous liquefaction depth (e.g., Qi and Gao, 2018) are limited to pure waves.

In the present study, the instantaneous liquefaction of a non-cohesive seabed under the combined wave-current loading is investigated analytically. The explicit solution for instantaneously-liquefied depth is derived and verified with degradation analyses and comparisons with existing offshore field observations. Parametric study is then performed

to examine the effects of wave nonlinearity and imposing a current.

2. Theoretical derivation

We consider a uniform current that is superimposed onto the progressive non-linear waves travelling along the porous seabed (see Fig. 1). As illustrated in Fig. 1, h is the water depth; L and H are the resulting wavelength and wave height, respectively; the steady current holds a velocity of U_c (note: the positive values of U_c are for a following current, and the negative ones are for an opposing current). Both the following and the opposing currents are considered to examine the combined wave-current induced instantaneous liquefaction of a non-

cohesive seabed. The instantaneously-liquefied seabed can be divided into the upper liquefied layer and the underlying un-liquefied zone (see Fig. 1).

2.1. Wave-current pressure at the mudline and pore pressure distribution within the liquefied layer

2.1.1. Combined 3rd order Stokes wave-current induced periodic pressure at the mudline ($z = 0$)

The analytical solution for the velocity potential in the Eulerian approach was derived by Chen and Juang (1990) for the 3rd order approximation of the periodic waves propagating over a uniform current. On the basis of Euler–Lagrange transformation, an updated 3rd order trajectory solution in Lagrangian form for the water particles in the wave-current interaction flow was later derived by Hsu et al. (2009). The velocity potential (φ) in the Eulerian coordinates approach for combined waves and a uniform current can be expressed as (Hsu et al., 2009):

$$\varphi(x,z,t) = U_c x + \frac{H}{2k}(\omega_0 - kU_c)\frac{\cosh(kz)}{\sinh(kh)}\sin(kx - \omega t)$$

$$\frac{3H^2}{32}(\omega_0 - kU_c)\frac{\cosh 2(kz)}{\sinh^4(kh)}\sin 2(kx - \omega t) - \frac{H^2}{16}(\omega_0 - kU_c)^2\frac{t}{\sinh^2(kh)} + \frac{kH^3}{512}(\omega_0 - kU_c)\frac{9 - 4\sinh^2(kh)}{\sinh^7(kh)}\cosh 3(kz)\sin 3(kx - \omega t) \tag{1}$$

Submitting the velocity potential (φ) into the Bernoulli's equation:

$$\frac{P}{\rho_f} + \frac{\partial \varphi}{\partial t} + \frac{1}{2}(\nabla\varphi)^2 + gz = 0 \tag{2}$$

the nonlinear wave-current induced periodic pressure on the seabed mudline ($P_b = P(x,z,t)|_{z=0}$) can be derived as

$$P_b = P_{b1} + P_{b2} + P_{b3} \tag{3}$$

in which, P_{b1}, P_{b2}, and P_{b3} are the 1st, 2nd, and 3rd order components of the total wave pressure, respectively:

$$P_{b1} = \frac{\rho_f gH}{2\cosh(kh)}\left[1 + \frac{\omega_2(kH)^2}{\omega_0 - kU_c}\right]\cos(kx - \omega t) \tag{4a}$$

$$P_{b2} = \frac{\rho_f gkH^2}{8\sinh(2kh)}\left[\frac{3}{\sinh^2(kh)}\left(1 + \frac{\omega_2(kH)^2}{\omega_0 - kU_c}\right) - 1\right]\cos[2(kx - \omega t)] \tag{4b}$$

$$P_{b3} = \frac{3\rho_f gk^2 H^3}{64\sinh^4(kh)\cosh(kh)}\left[\left(\frac{9 - 4\sinh^2(kh)}{8\sinh^2(kh)}\left(1 + \frac{\omega_2(kH)^2}{\omega_0 - kU_c}\right) - 1\right)\cos[3(kx - \omega t)] - \cos(kx - \omega t)\right] \tag{4c}$$

Under the Stokes 3rd order approximation, the terms higher than $O(H^3)$ should be omitted; thus Eqs. (4b) and (4c) can be further simplified as follows:

$$P_{b2} \approx \frac{\rho_f gkH^2}{8\sinh(2kh)}\left[\frac{3}{\sinh^2(kh)} - 1\right]\cos[2(kx - \omega t)] \tag{4b'}$$

$$P_{b3} \approx \frac{3\rho_f gk^2 H^3}{64\sinh^4(kh)\cosh(kh)}\left[\left(\frac{9 - 4\sinh^2(kh)}{8\sinh^2(kh)} - 1\right)\cos[3(kx - \omega t)] - \cos(kx - \omega t)\right] \tag{4c'}$$

In Eqs. (1)–(4), P is the water pressure; ρ_f is the water density; g is the gravitational acceleration; ω is the angular frequency for the combined wave-current, which is related to the wave number (k) by the following dispersion relationships obtained by perturbation analysis with taking "kH" as a minor term (Chen and Juang, 1990):

$$\omega = \omega_0 + (kH)^2\omega_2 \tag{5}$$

in which,

$$\omega_0 = U_c k + \sqrt{gk\tanh(kh)} \tag{6a}$$

$$\omega_2 = \frac{9 + 8\sinh^2(kh) + 8\sinh^4(kh)}{64\sinh^4(kh)}(\omega_0 - U_c k) \tag{6b}$$

Eq. (6a) is commonly referred to as the Doppler-shifted solution to the dispersion relation under combined linear waves and a uniform current (see Peregrine, 1976). Submitting Eqs. (6a) and (6b) into Eq. (5), and denoting
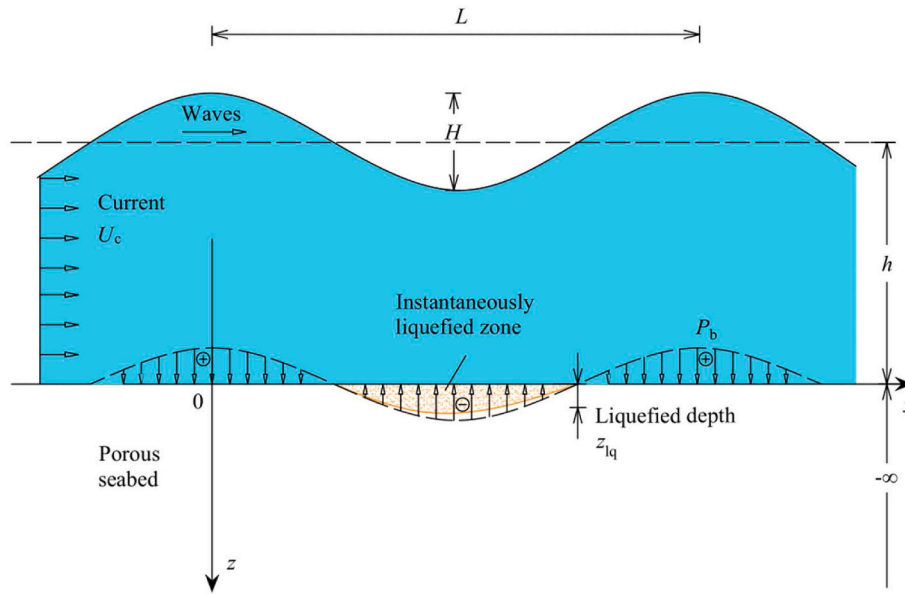
Fig. 1. Illustration of combined wave-current induced instantaneous liquefaction of a porous seabed.

$$\xi = \frac{9 + 8\,\sinh^2(kh) + 8\,\sinh^4(kh)}{64\,\sinh^4(kh)} \tag{7}$$

one can obtain the dispersion relationship for combined 3rd order Stokes waves and a uniform current:

$$\omega - U_c k = \left(1 + \xi(kH)^2\right)\sqrt{gk\,\tanh(kh)} \tag{8}$$

in which, "$\omega - U_c k$" is the relative angular frequency in the Lagrangian coordinates. By using Eq. (8), one can determine the wave number k or the wavelength L ($= 2\pi/k$), which would be further employed in the calculation for the P_b (see Eqs. (4a)-(4c)). As above stated, in the previous studies (Ye and Jeng, 2012; Zhang et al., 2013), the wave height (H) was assumed unchanged after the current is superimposed onto the waves; moreover, a different expression for the 3rd order component (P_{b3}) of P_b was derived, in which some minor terms were ignored. In fact, the wave-current combination would further change the original wave height (H_0) of pure waves as an updated wave height H, which can be evaluated with an analytical approximation (see Zou, 2004):

$$H = \left(\frac{k + 2kk_0h/\sinh(2k_0h)}{k_0[1 + 2kh/\sinh(2kh)] + 2U_c k_0\sqrt{k/g}\,\tanh(kh)}\right)^{\frac{1}{2}}H_0 \tag{9}$$

where k_0 is the wave number of the original waves without the current, which can be calculated by the dispersion relationship degraded from Eq. (8):

$$\omega = \left(1 + \xi(k_0H_0)^2\right)\sqrt{gk_0\,\tanh(k_0h)} \tag{10}$$

After superposing the current, the value of ω keeps unchanged; the wavelength and wave height of original waves (i.e., L_0 and H_0) would change to L and H, correspondingly. As observed by Qi et al. (2019), a following current onto the progressive waves can elongate the wavelength and diminish the wave height, while an opposing current can shorten the wavelength and magnify the wave height. Note that if the velocity of an opposing current exceeds a certain value, the resulting waves could break. The wave celerity v for the combined wave-current can be expressed as (Zou, 2004):

$$v = \frac{\tanh(kh)}{2\,\tanh(k_0h)}\left[1 + \left(1 + 4\frac{U_c}{v_0}\frac{\tanh(k_0h)}{\tanh(kh)}\right)^{\frac{1}{2}}\right]v_0 + U_c \tag{11}$$

in which, v_0 ($= \omega/k_0$) is the wave celerity of pure waves. To avoid wave

breaking, the range of current velocity U_c can be derived from Eq. (11):

$$U_c \geq -\frac{v_0}{4}\frac{\tanh(kh)}{\tanh(k_0h)} \tag{12}$$

2.1.2. Pore pressure distribution within the instantaneously-liquefied layer
   In the instantaneously-liquefied soil layer under wave troughs, the buoyant unit weight (γ') of the soil is balanced by the vertical gradient of excess pore pressure (i.e., criterion-III: $j_z - \gamma' \equiv 0$), so that the effective overburden stress vanishes (Qi and Gao, 2018). Similarly, under the action of combined wave-current loading, the excess pore pressure in the instantaneously-liquefied layer can be expressed as:

$$p(z) = P_b + \gamma' z \ \left(0 \leq z < z_{lq}\right) \tag{13}$$

where z_{lq} is the instantaneously-liquefied soil depth within the seabed, which is to be solved in Section 2.3.

2.2. Pore pressure distribution within the un-liquefied zone

2.2.1. Governing equations
   The underlying un-liquefied layer of the seabed is treated as an elastic, isotropic and homogeneous porous medium. Based on Biot's
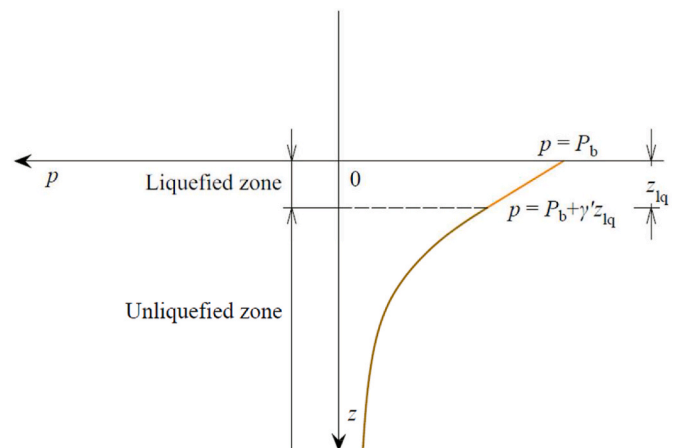

Fig. 2. Illustration of pore pressure distribution in the seabed with an instantaneous-liquefied layer.

consolidation theory (Biot, 1941), the continuity equation for the compressive pore fluid in a compressive porous medium for the two-dimensional problem can be expressed as:

$$\frac{k_s}{\gamma_w}\left(\frac{\partial^2 p}{\partial x^2}+\frac{\partial^2 p}{\partial z^2}\right)-n\beta\frac{\partial p}{\partial t}=\frac{\partial\varepsilon}{\partial t} \tag{14}$$

where k_s is the permeability coefficient of the soil; γ_w is the unit weight of the pore water ($\gamma_w = 9.8$ kN/m³); p is the excess pore pressure in the soil; n is the soil porosity; β is the compressibility of the pore fluid, i.e., $\beta = 1/K_f + (1-S_r)/p_{w0}$, in which K_f is the true bulk modulus of water ($K_f \approx 2.2\times10^9$Pa for the shallow water at 20ºC), S_r is the degree of saturation, and p_{w0} is the absolute pressure of the pore-water; ε is the volume strain of the soil under the plane strain condition, i.e., $\varepsilon = \partial u/\partial x + \partial w/\partial z$, in which u and w are the components of soil displacements in the horizontal and vertical directions, respectively. Based on the effective stress principle and Hooke's law, the equilibrium equations for a poro-elastic medium under the plane strain condition are as follows:

$$G\nabla^2 u+\frac{G}{(1-2\mu)}\frac{\partial\varepsilon}{\partial x}=\frac{\partial p}{\partial x} \tag{15a}$$

$$G\nabla^2 w+\frac{G}{(1-2\mu)}\frac{\partial\varepsilon}{\partial z}=\frac{\partial p}{\partial z} \tag{15b}$$

where G and μ are the shear modulus and Poisson's ratio of the soil, respectively; they are related with Young's modulus (E) by $G = E/2(1+\mu)$.

To derive the analytical solutions for combined wave-current induced transient pore pressure in the un-liquefied zone underneath the instantaneously-liquefied layer, the governing equations (Eq. (14), (15a)-(15b)) should be solved under the following boundary conditions.

2.2.2. Boundary conditions

(1) Pore pressure and effective stresses at the interface between the liquefied-layer and its underlying un-liquefied soil ($z = z_{lq}$):

Based on the continuity of pore pressure distribution (see Fig. 2), the excess pore pressure at the interface ($z = z_{lq}$) between the liquefied-layer and its underlying soil can be expressed from Eq. (13):

$$p(z)\big|_{z=z_{lq}}=P_b+\gamma' z_{lq} \tag{16}$$

where

$$\sigma_z'=2G\left(\frac{\partial w}{\partial z}+\frac{\mu\varepsilon}{1-2\mu}\right) \tag{18a}$$

$$\tau_{xz}=G\left(\frac{\partial u}{\partial z}+\frac{\partial w}{\partial x}\right) \tag{18b}$$

(2) Boundary conditions at the bottom of the seabed with an infinite thickness ($z\to\infty$):

Under the condition of the seabed thickness (T_b) much larger than the wavelength ($T_b\gg L$), the seabed can be assumed as a porous medium with an infinite depth. In the present analytical derivation, both the excess pore pressure and the corresponding soil displacements vanish while $z\to\infty$ (see Fig. 2):

$$p\big|_{z=\infty}=u\big|_{z=\infty}=w\big|_{z=\infty}=0 \tag{19}$$

2.2.3. Pore pressure response within the un-liquefied zone

Following the analytical framework by Madsen (1978), the forms of the excess pore pressure and the soil displacements in an un-liquefied layer ($z\ge z_{lq}$) can be expressed as follows:

$$\left\{\begin{matrix}p\\u\\w\end{matrix}\right\}=\sum_{m=1}^{3}P_m\mathrm{Re}\left\{\begin{bmatrix}P_1^{(m)}(z-z_{lq})\\U_1^{(m)}(z-z_{lq})\\W_1^{(m)}(z-z_{lq})\end{bmatrix}e^{im(kx-\omega t)}\right\} \tag{20}$$

in which the operator "Re{ }" means to take the real-part of the complex variable, and P_m is the corresponding " $\cos m\theta$" components of the seabed surface pressure P_b. Substituting Eq. (20) into the governing equations ((14), (15a)-(15b)) leads to the characteristic equation:

$$\left(D^2-m^2k^2\right)^2\left(D^2-\delta_m^2\right)U_1^{(m)}=0 \tag{21}$$

in which, $D=\partial/\partial z$ and

$$\delta_m^2=m^2k^2-\frac{im\omega\gamma_w}{k_s}\left(n\beta+\frac{1-2\mu}{2G(1-\mu)}\right) \tag{22}$$

The general solution of Eq. (21) can be expressed as:

$$U_1^{(m)}=\left(A_{1m}+A_{2m}(z-z_{lq})\right)e^{-mk(z-z_{lq})}+\left(A_{3m}+A_{4m}(z-z_{lq})\right)e^{mk(z-z_{lq})}+A_{5m}e^{-\delta_m(z-z_{lq})}+A_{6m}e^{\delta_m(z-z_{lq})} \tag{23a}$$

$$W_1^{(m)}=\left(B_{1m}+B_{2m}(z-z_{lq})\right)e^{-mk(z-z_{lq})}+\left(B_{3m}+B_{4m}(z-z_{lq})\right)e^{mk(z-z_{lq})}+B_{5m}e^{-\delta_m(z-z_{lq})}+B_{6m}e^{\delta_m(z-z_{lq})} \tag{23b}$$

$$P_1^{(m)}=\left(C_{1m}+C_{2m}(z-z_{lq})\right)e^{-mk(z-z_{lq})}+\left(C_{3m}+C_{4m}(z-z_{lq})\right)e^{mk(z-z_{lq})}+C_{5m}e^{-\delta_m(z-z_{lq})}+C_{6m}e^{\delta_m(z-z_{lq})} \tag{23c}$$

Both the effective normal stress (σ_z') and the shear stress (τ_{xz}) vanish at $z = z_{lq}$:

$$\sigma_z'\big|_{z=z_{lq}}=\tau_{xz}\big|_{z=z_{lq}}=0 \tag{17}$$

Substituting Eqs. (23a)-(23c) into the governing equations (Eq. (14), (15a)-(15b)) and the boundary conditions (Eqs. (16)-(17), (19)) gives the combined wave-current induced excess pore pressure in the un-liquefied soil layer ($z\ge z_{lq}$)):

$$p(z)=\sum_{m=1}^{3}\left\{\frac{P_m(1+A)}{1-2\mu}\left[(1-2\mu-\lambda_m)D_{2m}e^{-mk(z-z_{lq})}+\frac{\delta_m^2-m^2k^2}{mk}(1-\mu)D_{5m}e^{-\delta_m(z-z_{lq})}\right]e^{im(kx-\omega t)}\right\} \tag{24}$$

In Eq. (24), the coefficients A, λ_m, D_{2m} and D_{5m} are expressed as follows:

$$A = \frac{\gamma' z_{\mathrm{lq}}}{\sum\limits_{m=1}^{3} \left[P_m \mathrm{e}^{\mathrm{i}m(kx-\omega t)} \right]} \tag{25a}$$

$$\lambda_m = \frac{(1-2\mu)n\beta G}{n\beta G + (1-2\mu)} \tag{25b}$$

$$D_{2m} = \frac{\delta_m - \delta_m \mu + mk\mu}{\delta_m - \delta_m \mu + mk\mu + mk\lambda_m} \tag{25c}$$

$$D_{5m} = \frac{mk\lambda_m}{(\delta_m - mk)(\delta_m - \delta_m \mu + mk\mu + mk\lambda_m)} \tag{25d}$$

For the case of no liquefaction (i.e., $z_{\mathrm{lq}} = 0$), $A = 0$, then Eq. (24) can be degraded to the analytical solution by Zhang et al. (2013).

2.3. Analytical solutions of wave-current induced instantaneous liquefaction depth

Based on the above derivations (see Eqs. (13) and (24)), the wave-current induced pore-pressure distribution in the non-cohesive seabed with an instantaneously-liquefied layer can be unified with a piecewise function:

$$p(z) = \begin{cases} P_{\mathrm{b}} + \gamma' z & (0 \leq z < z_{\mathrm{lq}}) \\ \sum\limits_{m=1}^{3} \mathrm{Re} \left\{ \frac{P_m(1+A)}{1-2\mu} \left[(1-2\mu-\lambda_m) D_{2m} e^{-mk(z-z_{\mathrm{lq}})} + \frac{\delta_m^2 - m^2 k^2}{mk} (1-\mu) D_{5m} e^{-\delta_m(z-z_{\mathrm{lq}})} \right] \mathrm{e}^{\mathrm{i}m(kx-\omega t)} \right\} & (z \geq z_{\mathrm{lq}}) \end{cases} \tag{26}$$

As aforementioned, in the instantaneously-liquefied layer of the seabed, the vertical gradient of excess pore pressure should be identical to the buoyant unit weight of the soil (criterion-III, see Qi and Gao (2018)). The continuity of the derivative of pore pressures at the interface between the instantaneously-liquefied layer and its underlying soil should be satisfied (see Fig. 2):

$$\frac{\partial p}{\partial z} \bigg|_{z=z_{\mathrm{lq}}} = \gamma' \tag{27}$$

Substituting Eq. (24) into Eq. (27), the instantaneously-liquefied soil depth of a non-cohesive seabed under combined waves and current can be finally derived:

$$z_{\mathrm{lq}} = \frac{-1}{\mathrm{Re}\left(\sum\limits_{m=1}^{3} \varphi_m \xi_m \right)} - \frac{\mathrm{Re}\left(\sum\limits_{m=1}^{3} P_m \varphi_m \mathrm{e}^{\mathrm{i}m(kx-\omega t)} \right)}{\gamma' \mathrm{Re} \sum\limits_{m=1}^{3} \varphi_m \xi_m} \tag{28}$$

where

$$\varphi_m = \frac{1}{1-2\mu} \left(mk D_{2m}(1-2\mu-\lambda_m) + \frac{\delta_m^2 - m^2 k^2}{mk}(1-\mu)\delta_m D_{5m} \right) \tag{29a}$$

$$\xi_m = \frac{P_m \mathrm{e}^{\mathrm{i}m(kx-\omega t)}}{\sum\limits_{m=1}^{3} \left[P_m \mathrm{e}^{\mathrm{i}m(kx-\omega t)} \right]} \tag{29b}$$

Although completely instantaneous liquefaction generally occurs within the shallow soil layer, the pore-pressure distribution under the instantaneously-liquefied layer (see Eq. (26)) may reduce the effective stress, which should be well considered when evaluating the stability of

submarine structures (Qi and Gao, 2018).

3. Verification

To verify the derived solutions for combined wave-current induced instantaneously-liquefied depth, the degradation analyses and comparisons with existing offshore field observations are performed, respectively.

3.1. Degradation analyses

If only linear waves are taken into account, the velocity of current (U_c), the 2nd and the 3rd order nonlinear components of the total wave pressure (see Eqs. (4a)-(4c)) would all approach zero, i.e., $U_c = 0$, $P_2 \to 0$, $P_3 \to 0$. The minor term "kH" in Eq. (4a) for perturbation analyses can be further omitted. As such, the wave number k would be equal to k_0; and the wave height H would be equal to H_0 (note: the subscript "0" denotes the parameters without superposing a current). Thus, the derived instantaneously-liquefied soil depth (Eq. (28)) can be simplified as

$$z_{\mathrm{lq}} = \frac{-P_0 \mathrm{Re}\left[\varphi_1 \mathrm{e}^{\mathrm{i}(k_0 x-\omega t)} \right]}{\gamma' \mathrm{Re}(\varphi_1)} - \frac{1}{\mathrm{Re}(\varphi_1)} \quad \text{(for pure linear waves)} \tag{30}$$

in which P_0 is the amplitude of the excess pore pressure at the seabed mudline under pure linear wave loading, i.e., $P_0 = \gamma_{\mathrm{w}} H_0 /(2\cosh(k_0 h))$.

An analytical solution for pure wave-induced instantaneous liquefaction depth was recently derived by Qi and Gao (2018) as follows:

$$z_{\mathrm{lq}} = \frac{-P_0 \cos(k_0 x - \omega t)}{\gamma'} - \frac{1}{\mathrm{Re}[k_0(1-\alpha) + \delta_1 \alpha]} \tag{31}$$

in which δ_1 can be calculated with Eq. (22) for $m = 1$; and

$$\alpha = \frac{\mathrm{i}M\omega''}{\mathrm{i}(1+M)\omega'' + \delta'} \tag{32}$$

where $M = n\beta G /(1-2\mu)$, $\omega'' = (1-\mu)\omega' /[(1-2\mu)k_0^2]$, $\delta' = (\delta_1 - k_0)/k_0$, $\omega' = \omega/c$, $c = k_{\mathrm{s}}\{\gamma_{\mathrm{w}}[n\beta + (1-2\mu)/2(1-\mu)G]\}^{-1}$. Comparing Eq. (29a) with Eq. (32), one can find $\varphi_1 = k_0(1-\alpha) + \delta_1 \alpha$. Thus, Eq. (31) can be further expressed as:

Table 1
Input data for the comparisons.

Parameters		Values
Seabed properties	Degree of saturation S_{r} (%)	98.0
	Coefficient of permeability k_{s} (m/s)	1×10^{-4}
	Elastic modulus E (MPa)	30.0
	Porosity of soil n	0.45
	Poisson ratio of soil μ	0.30
	Submerged unit weight of soil γ' (kN/m^3)	8.82
Wave parameters	Water depth h (m)	10.0
	Wave height H_0 (m)	3.0
	Wave period T (s)	Varied from 6.0 to 10.0

(a)

(b)
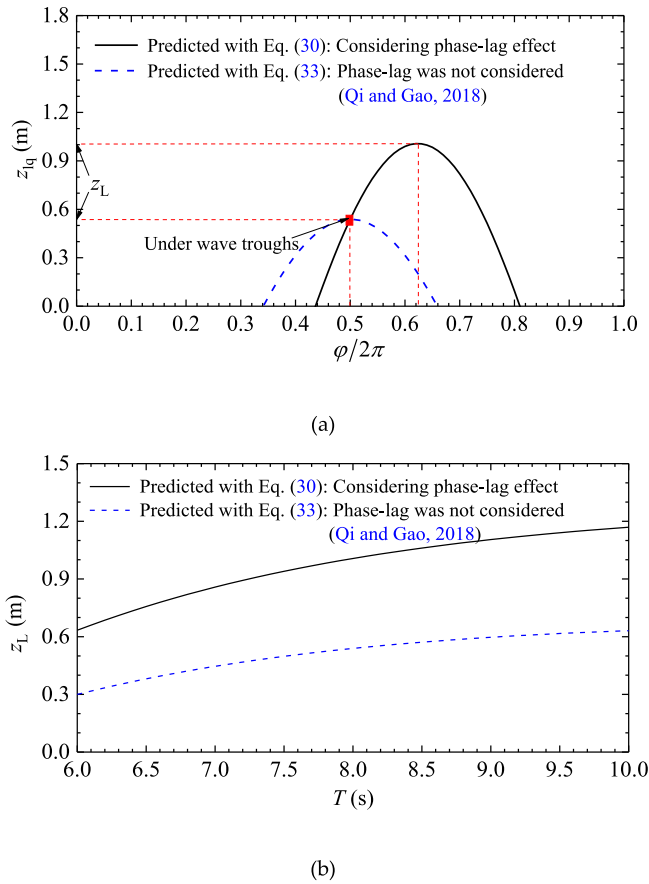
Fig. 3. Phase-lag effect on the instantaneously-liquefied depth: (a) variation of z_{lq} with $\varphi/2\pi$ (for $T = 8.0$ s); (b) variation of z_L with T.

$$z_{lq} = \frac{-P_0 \mathrm{Re}\left(e^{i(k_0 x - \omega t)}\right)}{\gamma'} - \frac{1}{\mathrm{Re}(\varphi_1)} \tag{33}$$

It should be noticed that, although the degraded solution Eq. (30) has a similar form with Eq. (33) by Qi and Gao (2018), there exists a difference between their first items due to different assumptions. That is, in the solution by Qi and Gao (2018), the phase-lag of pore pressure was neglected. In the present derivations, we assume that $p = \sum_{m=1}^{3} P_m \mathrm{Re}[P_1^{(m)}(z - z_{lq}) e^{im(kx - \omega t)}]$ (see Eq. (20)) instead of $p = \sum_{m=1}^{1} P_m \mathrm{Re}[P_1^{(m)}(z - z_{lq})] \cos(kx - \omega t)$, so that the phase-lag can be taken into account.

In the scenario of wave/current-seabed interactions, the pore pressure attenuation within a porous seabed is usually accompanied by phase lag, which has been observed in wave flumes (e.g., for the pure wave loading by Tsui and Helfrich (1983); for the combined wave-current loading by Qi et al. (2019)) and in-situ measurements (e. g., Maeno and Hasegawa, 1987). The phase lag refers to a phenomenon that the phase of pore pressure fluctuations at certain soil depths within the seabed usually lags behind the initial phase of wave pressure at the mudline while the periodic waves propagating along the seabed. As aforementioned, numerous analytical solutions for wave-seabed interactions have been developed (e.g., Moshagen and Tørum, 1975; Yamamoto et al., 1978; Madsen, 1978; Mei and Foda, 1981; Okusa,

1985; Hsu and Jeng, 1994; Jeng et al., 2007; Zhang et al., 2013). In the previous analytical solutions, the phase lag was implicitly involved in their derivations. It has been recognized that the degree of saturation of the soil plays a very important role for pore pressure attenuation, especially in the very fine sediments (see, Hsu and Jeng, 1994). Based on the analytical solution by Yamamoto et al. (1978), an explicit expression for phase lag was recently derived by Li and Gao (2022), which matches well with their flume observations. It was indicated that the phase lag and the amplitude attenuation are closely correlated, which are both influenced by the wave parameters (including wave period T, and wave number k) and the soil properties (especially for the permeability and the compressibility of soils).

To examine the effects of phase-lag on the instantaneously-liquefied soil depth, a parametric study is further made for comparisons between the present solution (Eq. (30)) and the previous solution (Eq. (33)). The input data for soil properties and wave parameters are listed in Table 1.

The variations of the wave-induced instantaneously-liquefied soil depth (z_{lq}) with its corresponding phase ($\varphi/2\pi$) are shown in Fig. 3(a). Due to the existence of phase-lag (see Mei and Foda, 1981; Hsu and Jeng, 1994), the maximum value of pore pressure gradient no longer emerges exactly under wave troughs, and the maximum instantaneously-liquefied soil depth (z_L) no longer emerges exactly under wave troughs consequently (see Fig. 3(a)). The value of z_L predicted with Eq. (30) in the present degraded solution considering phase-lag becomes almost twice of the predicted value with Eq. (33), indicating the phase-lag effect is not ignorable in predicting z_L. As illustrated in Fig. 3(b), with the increase of wave period from $T = 6.0$ s–10.0 s, the phase-lag effect on the instantaneously-liquefied soil depth gets much more significant.

3.2. Comparisons with existing offshore field observations

In this section, the present analytical solution is compared with the offshore field observations, which were carried out at the Hazaki Oceanographical Research Facility (HORF) in Japan intermittently for two years between 1988 and 1989 (Zen and Yamazaki, 1991). The HORF is located at Hazaki in Ibaraki prefecture (facing the Pacific Ocean), which extends 427 m offshore from the shoreline to enable the observation of waves, currents, and other marine phenomena even in rough sea. The field observation was performed at the tip of HORF where the water depth varied between 4.0 m and 6.0 m. In their field observation, five pore pressure gauges (full range of 343 kPa with a precision of 0.5%) were installed at 0.5 m intervals in the vertical direction of the seabed to measure the pore pressure response at various depths. Two earth press gauges (full range of 196 kPa with a precision of 0.5%) were utilized to monitor the vertical earth pressure, and another two were used to measure the horizontal earth pressure. Meanwhile, an ultrasonic wave gauge was located on the deck to record the wave height and wave period. The physical properties of the Hazaki sand at the seabed are shown in Table 2.

Fig. 4 shows the records of horizontal total stress variation ($\Delta\sigma_h$) at various depths within the seabed during the Series No. 3 observation on April 24, 1989. It was observed that there exist high frequency fluctuations of $\Delta\sigma_h$ (highlighted by the dotted circles for waves Nos. 27–28, Nos. 29–30, and Nos. 32–33, respectively, see Fig. 4(a)) monitored by the horizontal earth pressure gauge which was buried in the shallow depth ($z = 0.32$ m); nevertheless, the measure values of $\Delta\sigma_h$ at the deeper depth ($z = 1.06$ m) kept more continuous and smoother (see Fig. 4(b)). Zen and Yamazaki (1991) speculated that such phenomenon

Table 2

Physical properties of Hazaki sand from the shallow deposits at HORF (Zen and Yamazaki, 1991).

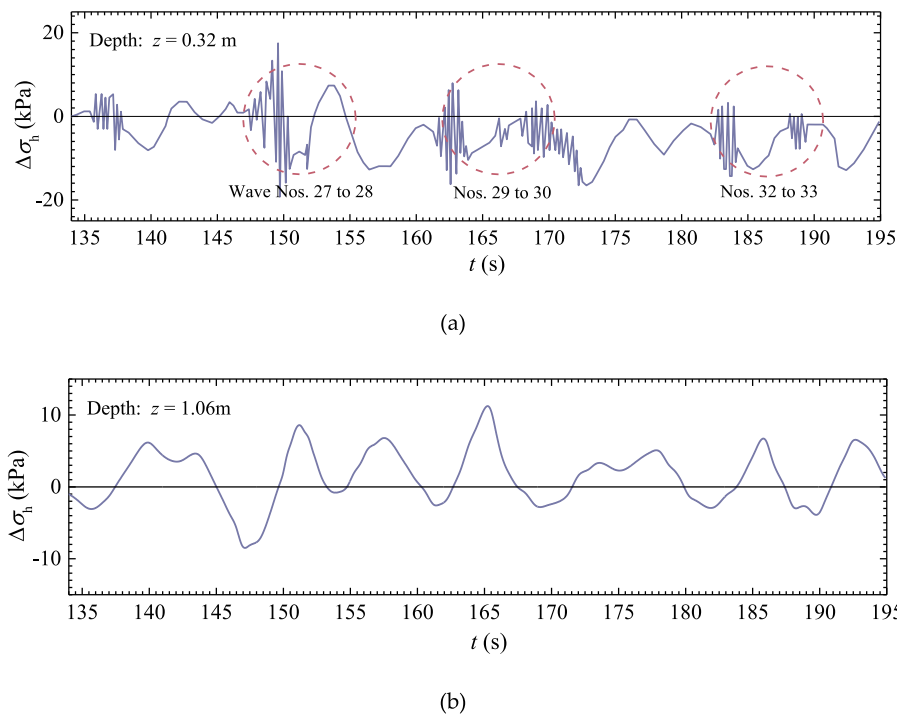| Specific gravity	Buoyant unit weight	Void ratio	Elastic modulus	Poisson ratio	Coefficient of permeability	Degree of saturation
G_s	γ' (kN/m³)	e	E (MPa)	μ	k_s (m/s)	S_r (%)
2.69	9.50	0.75	42.5	0.33	1.12×10^{-4}	99.45

(a)

(b)

Fig. 4. The records of horizontal total stress variation during the Series No. 3 observation: (a) z = 0.32 m; (b) z = 1.06 m (Adapted from Zen and Yamazaki (1991)).
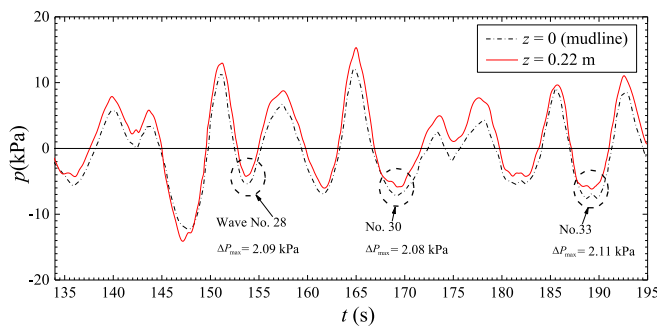

Fig. 5. The measured wave pressure at the mudline ($z = 0$) and the pore pressure within the seabed ($z = 0.22$ m) during the Series No. 3 observation (Adapted from Zen and Yamazaki (1991)).

of high frequency fluctuations was caused by the occurrence of instantaneous liquefaction in the shallow layer of the seabed, i.e., the hydrodynamic pressure induced by the liquefied state of soil elements led to the noise-like high frequency fluctuations. It was indicated that the maximum instantaneous liquefaction depth (z_L) during the three wave events could be between 0.32 m and 1.06 m (i.e., $0.32 m \leq z_L < 1.06 m$). Fig. 5 gives the measured wave pressure at the mudline ($z = 0$) and the pore pressure within the seabed ($z = 0.22$ m), respectively. During the seabed instantaneous liquefaction events for the Wave No. 28, 30, and 33 (see Fig. 5), the corresponding maximum values of the pore pressure

difference (ΔP_{max}) in the negative pressure zone beneath wave troughs are ΔP_{max} = 2.09, 2.08, and 2.11 (kPa), respectively.

For comparisons between the offshore field observations and present analytical predictions, the wave parameters of the Waves Nos. 28, 30, and 33 during the Series No. 3 observations by Zen and Yamazaki (1991) are given in Table 3. The field measured values of the pore pressure difference (ΔP_{max}) between the seabed mudline (i.e., $z = 0$) and $z = 0.22$ m, and the ranges of maximum instantaneous liquefaction depth (z_L) are also listed in Table 3.

Once the values of wave parameters and soil properties (see Tables 2 and 3) are given, the wave-induced instantaneous liquefaction depth can be obtained analytically with Eq. (28). Note that, the field observation and analyses by Zen and Yamazaki (1991) indicated that, the soil layer detected by the earth pressure gauge buried at $z = 0.32$ m was liquefied, but the soil layer detected by another earth pressure gauge at $z = 1.06$ m was un-liquefied (see Fig. 4(a) and (b)). As shown in Table 3, the predicted values of z_L are generally within the range of the offshore field measurements, i.e., $0.32 m \leq z_L < 1.06 m$. As aforementioned, for an instantaneously-liquefied soil layer, the vertical gradient of excess pore pressure ($\partial p/\partial z$) should be identical to the buoyant unit weight of the soil (γ'), i.e., $\partial p/\partial z = \gamma'$. In their offshore field measurements, $\partial p/\partial z \approx \Delta P_m/\Delta z$, where the pore pressure was measured at $z = 0$ and 0.22 m, respectively (i.e., $\Delta z = 0.22$ m). The measured dry unit weights of the Hazaki sand from the shallow deposits at HORF were between 14.6–15.5 kN/m³, so the values of γ' were between 9.17–9.68 kN/m³. Thus, the predicted values of ΔP_m ($\approx \gamma' \Delta z$) between $z = 0$ and 0.22 m

Table 3
Wave parameters for the seabed instantaneous liquefaction events at HORF (Zen and Yamazaki, 1991), and the comparisons between the field observations and present analytical predictions.
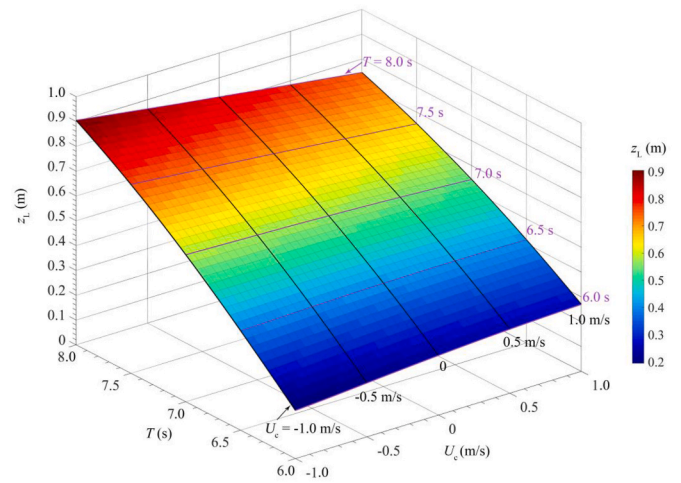
Wave Nos.	Wave parameters			ΔP_{max} (kPa) (between z = 0 and 0.22 m)		z_L (m)	
	T (s)	h (m)	H (m)	Field measured	Predicted	Field measured	Predicted
No. 28	5.25	4.85	2.31	2.09	2.02–2.13	0.32–1.06	0.44
No. 30	8.10	4.85	1.92	2.08			0.55
No. 33	7.20	4.85	1.95	2.11			0.35

Table 4
Input data of seabed properties and wave-current parameters for the parametric study.

Parameters		Values
Seabed properties	Degree of saturation S_r (%)	98.0
	Coefficient of permeability k_s (m/s)	1×10^{-4}
	Elastic modulus E (MPa)	30.0
	Porosity n	0.45
	Poisson ratio μ	0.30
	Buoyant unit weight γ' (kN/m³)	8.20
Wave-current parameters	Water depth h (m)	16.0
	Wave height H_0 (m)	Varied (3.0, 3.3, 3.6)
	Wave period T (s)	Varied (6.0–8.0)
	Current velocity U_c (m/s)[a]	−1.0–1.0

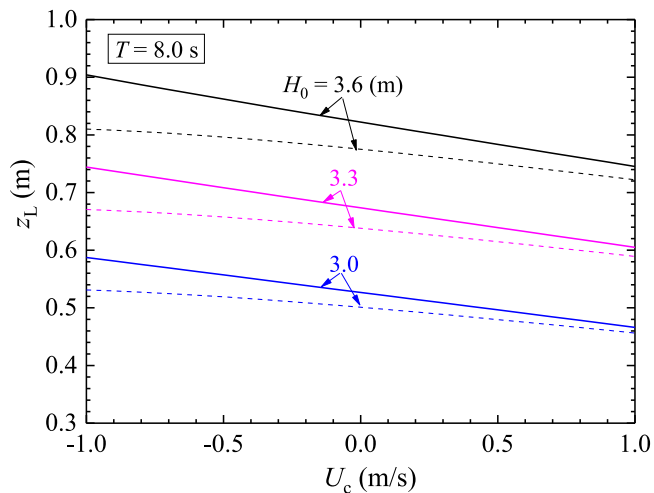[a] Note: the positive values of U_c are for a following current, and the negative ones are for an opposing current.


(a)

(b)

Fig. 6. Variations of maximum instantaneous liquefaction depth (z_L) with the current velocity (U_c) for various values of wave height (H_0) ($h = 16.0$ m): (a) $T = 6.0$ s; (b) $T = 8.0$ s (Solid lines: 3rd order Stokes wave-current interactions; Dash lines: linear wave-current interactions).

Fig. 7. Envelope for variation of maximum instantaneous liquefaction depth (z_L) with wave period (T) and current velocity (U_c) ($h = 16.0$ m, $H_0 = 3.6$ m).

(a)   (b)
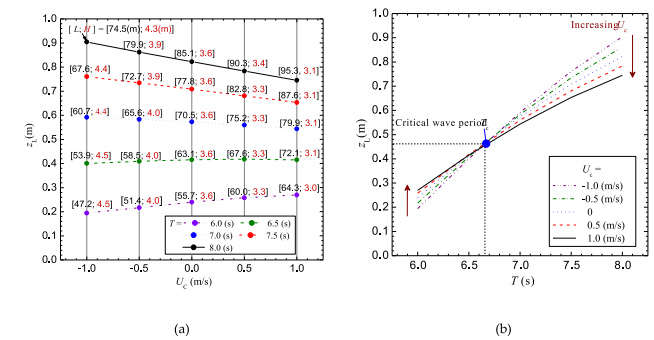
Fig. 8. 2D projections of the 3D envelope in Fig. 7: (a) z_L vs. U_c for various wave periods (T); (b) z_L vs. T for various current velocities (U_c) ($h = 16.0$ m, $H_0 = 3.6$ m).

would be in the range of 2.02–2.13 kPa, which match well with the field observations (see Table 3).

4. Parametric study: Effects of wave nonlinearity and superimposing a current

Parametric study is performed to examine the effects of wave nonlinearity and superimposing a current onto the progressive waves. The input data of seabed properties and wave-current parameters are listed in Table 4. The examined cases are for the combinations between a following or opposing current and the waves with relatively large wave steepness, which generally fall within the non-linear Stokes wave range (Hattori, 1987). To avoid wave breaking during the wave-current interactions, the velocity of an opposite current should not exceed a critical value: $U_{cb} = -0.25 v_0 \tanh(kh)/\tanh(k_0 h)$ (i.e., Eq. (12), see Section 2.1.1). Submitting the wave and current parameters into Eq. (12), one can obtain $U_{cb} = -1.94$ m/s. Thus, in the examined range of U_c (i.e., -1.0 m/s $\leq U_c \leq 1.0$ m/s, see Table 4), wave breaking can be avoided during wave-current interactions.

Variations of the maximum instantaneous liquefaction depth (z_L) predicted by the present solution (Eq. (28)) with the velocity of the imposing current (U_c) are obtained for the wave period $T = 6.0$ s (see Fig. 6(a)) and 8.0 s (see Fig. 6(b)), respectively. Various values of the wave height (H_0) for 3rd order Stokes waves are examined, i.e., $H_0 = 3.0$ m, 3.3 m, and 3.6 m. The corresponding values of z_L estimated with the degraded solution for the linear wave-current interaction are also shown with dash lines in Fig. 6. Note that, the degraded solution for the linear

wave-current interaction has the similar form to Eq. (30) considering pure linear waves, but here the wavenumber and wave height should be the updated values k (calculated from the degraded form of Eq. (6a)) and H (Eq. (9)) after wave-current interaction. It is indicated that the variation trends of z_L with U_c are similar for the non-linear and the linear solutions. As can be expected, for a given value of U_c, the values of z_L increase with the rise of H_0. Nevertheless, the solution for the 3rd order Stokes wave-current combination generally gives larger predictions of z_L than the linear solution. As illustrated in Fig. 6(a) and (b), the distinctions between these two solutions become much more pronounced when the wave height H_0 gets larger and the current velocity U_c is reduced. It is implied that wave-nonlinearity effects on the instantaneous liquefaction depth are not neglectable, i.e., the instantaneous liquefaction depth could be underestimated with the linear solution.

Moreover, the values of z_L increase nonlinearly with the rise of U_c for $T = 6.0$ s (see Fig. 6(a)), indicating that superimposing an opposing current could be beneficial for the prevention of instantaneous liquefaction (e.g., under the conditions of $T = 6.0$ s, $H_0 = 3.0$ m; $U_c = -0.95$ m/s, see Fig. 6(a)). It is interesting to notice that the values of z_L decrease with the increase of U_c for $T = 8.0$ s (see Fig. 6(b)), which exhibits a reverse effect on the instantaneous liquefaction depth as indicated in Fig. 6(a) for $T = 6.0$ s. In other words, the variations of z_L with U_c could be monotonic increasing for relatively small wave periods (see Fig. 6(a)), but decreasing for large wave periods (see Fig. 6(b)).

To clarify the influences of wave period (T) and current velocity (U_c) on maximum instantaneous liquefaction depth (z_L), the three-dimensional (3D) envelope for the variation of z_L with both T and U_c is constructed, as shown in Fig. 7. For more details, Fig. 8(a)-(b) further demonstrate the 2D projections of the 3D envelope, i.e., the variation of z_L with U_c for different values of T (= 6.0, 6.5, 7.0, 7.5, 8.0 (s), see Fig. 8(a)), and the variation of z_L with T for different values of U_c (= −1.0, −0.5, 0, 0.5, 1.0 (m/s), see Fig. 8(b)), respectively.

In the variations of z_L with U_c (see Fig. 8(a)), the corresponding values of wavelength (L) and wave height (H) are provided for certain values of U_c (= −1.0, −0.5, 0, 0.5, 1.0 (m/s)) and T (= 6.0, 6.5, 7.0, 7.5, 8.0 (s)). It is indicated that the increase of U_c would enlarge the wavelength (L) and simultaneously reduce the wave height (H) of the combined wave-current. For a fixed value of H, the enlargement of L would amplify the wave loading on the seafloor, which can result in an increase of instantaneous liquefaction depth; nevertheless, the decrease of H has a reversed effect, i.e., the instantaneous liquefaction depth is reduced accordingly. There seems exist a critical wave period T_c ($\approx$6.65 s, see Fig. 8(b)), at which the effect of U_c on z_L could be ignorable, i.e., superimposing a current onto the progressive waves has a slight effect on instantaneous liquefaction depth. When $T < T_c$, the values of z_L are amplified with increasing U_c, and such amplification becomes much more significant for smaller wave periods (T); Conversely, when $T > T_c$, the values of z_L are reduced with increasing U_c, especially for larger values of T. That is, for the relatively small wave period (e.g., $T = 6.0$ s), the influence of wavelength enlargement dominates with increasing U_c, so that the instantaneous liquefaction depth z_L is increased. But for the relatively large wave period (e.g., $T = 8.0$ s), the reduction of wave height plays a dominant role for the decrease of z_L with increasing U_c. It can be recognized that, the variation trends of z_L with U_c and T are mainly attributed to the synthetical effects from the alterations of

wavelength (L) and wave height (H) while superimposing a current onto the waves.

5. Conclusions

In coastal environments, the periodic waves are frequently coexisting and coupled with an ocean current. Previous studies on the instantaneous liquefaction of the seabed were predominantly limited to pure wave conditions. Nevertheless, superposing a following or opposite current onto the progressive waves could significantly alter the excess pore-water pressures within the seabed. In the present study, the instantaneous liquefaction of a non-cohesive seabed under the combined 3rd order Stokes waves and a current is investigated analytically. The following conclusions can be drawn:

(1) Theoretical solutions for the excess pore pressure distribution and the corresponding instantaneous liquefaction depth are derived by adopting the third-order approximation of nonlinear wave-current interactions. The explicit solutions are verified by degradation analyses and comparisons with the existing offshore field observations.

(2) Parametric study is then performed to examine the effects of wave nonlinearity and superimposing a current onto the progressive waves. It is indicated that the wave-nonlinearity effects on the instantaneous liquefaction depth are not neglectable in the examined range of waves, i.e., the instantaneous liquefaction depth would be underestimated with the degraded linear wave-current solution.

(3) The envelope for the variation of maximum instantaneous liquefaction depth with both wave period and current velocity is further constructed. It is indicated that superimposing an opposing current onto the progressive waves with a relatively small wave period could be beneficial for the prevention of instantaneous liquefaction. Nevertheless, the variation trends of the maximum instantaneous liquefaction depth depend on the synthetical effect of the alternations of both wavelength and wave height due to wave-current interactions.

Author contributions

Li-Jing Yang: Writing—original draft preparation, Derivations, Data analyses; Fu-Ping Gao: Conceptualization, Writing-reviewing and editing, Supervision; Chang-Fei Li: Validation, Data analyses. All authors have read and agreed to the submitted version of the manuscript.

Declaration of competing interest

The authors declare that they have no known competing financial interests or personal relationships that could have appeared to influence the work reported in this paper.

Acknowledgements

Nomenclature

A	Coefficient in Eq. (24)
A_{nm} ($n = 1,2,3$)	Coefficients in Eq. (23)
B_{nm} ($n = 1,2,3$)	Coefficients in Eq. (23)
c	Coefficient in Eq. (32)
C_{nm} ($n = 1,2,3$)	Coefficients in Eq. (23)
$C(t)$	Bernoulli's constant

D	Derivative of z
D_{2m}, D_{5m}	Coefficients in Eq. (24)
e	Void ratio
E	Young's modulus of the soil
g	Gravitational acceleration
G	Shear modulus of the soil
G_s	Specific gravity
h	Water depth
H_0	Wave height of the pure wave
H	Wave height of the combined wave-current
i	Imaginary number
k_0	Wave number of the pure wave
k	Wave number of the combined wave-current
k_s	Coefficient of permeability
K_f	True bulk modulus of water
L	Wavelength of the combined wave-current
M	Coefficients in Eq. (32)
n	Soil porosity
p	Excess pore pressure in the soil
p_{w0}	Absolute static pressure
P	Water pressure
P_b	Excess pore pressure at the seabed surface
P_{bm}	The mth order components of seabed surface wave pressure P_b
P_m	the $\cos m\theta$ components of seabed surface wave pressure P_b
$P_0\ P_1^{(m)}$	Amplitude of excess pore pressure at seabed surface for linear wave
P_0	Functions of z in Eq. (20)
S_r	Degree of saturation
t	Time
T	Wave period
T_b	Sediment thickness of the seabed
u	Soil displacement in horizontal direction
$U_1^{(m)}$	Functions of z in Eq. (20)
U_c	Current velocity
U_{cb}	Critical current velocity for wave breaking
v_0	The wave velocity of the only wave
v	The wave velocity of the combined wave-current
w	Soil displacement in vertical direction
$W_1^{(m)}$	Functions of z in Eq. (20)
z_{lq}	Instantaneous liquefaction depth
z_L	Maximum instantaneous liquefaction depth
β	Compressibility of pore-fluid
ρ_f	Water density
ω	Angular frequency of the wave
ω_0, ω_2	Coefficients in Eq. (5)
ω', ω''	Coefficients in Eq. (32)
α	Coefficient in Eq. (31)
ε	Volume strain
γ'	Buoyant unit weight of soil
γ_w	Unit weight of water
μ	Poisson's ratio
φ	Velocity potential
η	Free surface elevation of the water
σ_z'	Effective normal stress in vertical direction
τ_{xz}	Shear stress
δ_m	Coefficients in Eq. (21)
δ'	Coefficients in Eq. (32)
λ_m	Coefficients in Eq. (24)
φ	Wave phase
φ_m	Coefficients in Eq. (28)
ξ	Coefficient in Eq. (7)
ξ_m	Coefficients in Eq. (28)
$\Delta\sigma_h$	Horizontal total stress variation
ΔP_{max}	Maximum pore-pressure difference

References

Baddour, R.E., Song, S.W., 1990. On the interaction between waves and currents. Ocean Eng. 17, 1–21.

Bear, J., 1972. Dynamics of Fluids in Porous Media. Courier Dover Publications, Dove.

Biot, M.A., 1941. General theory of three-dimensional consolidation. J. Appl. Phys. 12, 155–164.

Biot, M.A., 1956. Theory of propagation of elastic waves in a fluid-saturated porous solid. I. Low-frequency range. J. Acoust. Soc. Am. 28 (2), 168–177.

Chen, Y.Y., Juang, W.J., 1990. Primary analysis on wave-current interaction. In: Proc. 12th Conf. On Ocean Engng, pp. 248–265.

Christian, J.T., Taylor, P.K., Yen, J.K.C., 1974. Large diameter underwater pipeline for nuclear power plant designed against soil liquefaction. Houston. In: Proceedings of the 6th Annual Offshore Technology Conference, pp. 597–606.

De Groot, M.B., Kudella, M., Meijers, P., Oumeraci, H., 2006. Liquefaction phenomena underneath marine gravity structures subjected to wave loading. J. Waterw. Port, Coast. Ocean Eng. 132, 325–335.

Duan, L.L., Jeng, D.S., Wang, D., 2019. PORO-FSSI-FOAM: seabed response around a mono-pile under natural loadings. Ocean Eng. 184, 239–254.

Gao, F.P., Jeng, D.S., Sekiguchi, H., 2003. Numerical study on the interaction between non-linear wave, buried pipeline and non-homogenous porous seabed. Comput. Geotech. 30 (6), 535–547.

Hattori, M., 1987. Experimental study on the validity range of various wave theories. Coast. Eng. 232–246.

Hsu, H.C., Chen, Y.Y., Hsu, J.R.C., Tseng, W.J., 2009. Nonlinear water waves on uniform current in Lagrangian coordinates. J. Nonlinear Math. Phys. 6 (1), 47–61.

Hsu, J.R.C., Jeng, D.S., 1994. Wave-induced soil response in an unsaturated anisotropic seabed of finite thickness. Int. J. Numer. Anal. Methods GeoMech. 18 (11), 785–807.

Jeng, D.S., 1997. Wave-Induced Seabed Response in Front of a Breakwater. PhD Thesis. University of Western Australia, Perth.

Jeng, D.S., 2018. Mechanics of Wave-Seabed-Structure Interactions: Modeling, Processes and Applications. Cambridge University Press, Cambridge.

Jeng, D.S., Seymour, B., Gao, F.P., Wu, Y.X., 2007. Ocean waves propagating over a porous seabed: residual and oscillatory mechanisms. Sci. Chin. Series E Technol. Sci. 50 (1), 81–89.

Jensen, B., Christensen, E.D., Sumer, B.M., 2014. Pressure-induced forces and shear stresses on rubble mound breakwater armour layers in regular waves. Coast. Eng. 91, 60–75.

Judd, A., Hovland, M., 2007. Seabed Fluid Flow: the Impact on Geology, Biology and the Marine Environment. Cambridge University Press, p. 475.

Li, C.F., Gao, F.P., 2022. Characterization of spatio-temporal distributions of wave-induced pore pressure in a non-cohesive seabed: amplitude-attenuation and phase-lag. Ocean Eng. 253, 111315.

Li, C.F., Gao, F.P., Yang, L.J., 2021. Breaking-wave induced transient pore pressure in a sandy seabed: flume modeling and observations, 2021 J. Mar. Sci. Eng. 9 (2), 160.

Li, X.J., Gao, F.P., Yang, B., Zang, J., 2011. Wave-induced pore pressure responses and soil liquefaction around pile foundation, 2011 Int. J. Offshore Polar Eng. 21 (3), 233–239.

Li, Y.Z., Ong, M.C., Tang, T., 2020. A numerical toolbox for wave-induced seabed response analysis around marine structures in the OpenFOAM® framework. Ocean Eng. 195, 106678.

Lin, Z.B., Pokrajac, D., Guo, Y.K., Jeng, D.S., Tang, T., Rey, N., Zheng, J.H., Zhang, J.S., 2017. Investigation of nonlinear wave-induced seabed response around mono-pile foundation. Coast. Eng. 121, 197–211.

Longuet-Higgins, M.S., Stewart, R.W., 1960. Changes in the form of short gravity waves on long waves and tidal currents. J. Fluid Mech. 8, 565–583.

Longuet-Higgins, M.S., Stewart, R.W., 1961. The changes in amplitude of short gravity waves on steady non-uniform currents. J. Fluid Mech. 10, 529–549.

Madsen, O.S., 1978. Wave-induced pore pressures and effective stresses in a porous bed. Geotechnique 28 (4), 377–393.

Mase, H., Sakai, T., Sakamoto, M., 1994. Wave-induced porewater pressures and effective stresses around breakwater. Ocean Eng. 21 (4), 361–379.

Mei, C.C., Foda, M.A., 1981. Wave-induced responses in a fluid-filled poro-elastic solid with a free surface—a boundary layer theory. Geophys. J. Int. 66 (3), 597–631.

Maeno, Y., Hasegawa, T., 1987. In-situ measurements of wave-induced pore pressure for predicting properties of seabed deposits. Coast. Eng. Jpn. 30 (1), 99–115.

Michallet, H., Mory, M., Piedra-Cueva, I., 2009. Wave-induced pore pressure measurements near a coastal structure. J. Geophys. Res.: Oceans 114, C06019.

Miyamoto, T., Yoshinaga, S., Soga, F., 1989. Seismic prospecting method applied to the detection of offshore breakwater units setting in the bed. Coast Eng. J. 32, 103–112.

Miyamoto, J., Sassa, S., Tsurugasaki, K., Sumida, H., 2019. Wave-induced liquefaction and floatation of a pipeline in a drum centrifuge. J. Waterw. Port, Coast. Ocean Eng. 146 (2), 04019039.

Miyamoto, J., Sassa, S., Tsurugasaki, K., Sumida, H., 2021. Wave-induced liquefaction and instability of offshore monopile in a drum centrifuge. Soils Found. 61 (1), 35–49.

Mory, M., Michallet, H., Bonjean, D., et al., 2007. A field study of instantaneous liquefaction caused by waves around a coastal structure. J. Waterw. Port, Coast. Ocean Eng. 133 (1), 28–38.

Moshagen, H., Tørum, A., 1975. Wave induced pressures in permeable seabeds. J. Waterw. Harbors Coast. Eng. Div. 101 (1), 49–57.

Okusa, S., 1985. Wave-induced stresses in unsaturated submarine sediments. Geotechnique 35 (4), 517–532.

Peregrine, D.H., 1976. Interaction of water waves and currents. Adv. Appl. Mech. 16, 9–117.

Qi, W.G., Gao, F.P., 2018. Wave induced instantaneously-liquefied soil depth in a non-cohesive seabed. Ocean Eng. 153, 412–423.

Qi, W.G., Gao, F.P., Han, X.T., Gong, Q.X., 2012. Local scour and pore-water pressure around a monopile foundation under combined waves and currents. Rhodes, Greece. In: Proceedings of the 22nd International Offshore and Polar Engineering Conference, pp. 159–165.

Qi, W.G., Li, C.F., Jeng, D.S., Gao, F.P., Liang, Z.D., 2019. Combined wave-current induced excess pore-pressure in a sandy seabed: flume observations and comparisons with theoretical models. Coast. Eng. 147, 89–98.

Qi, W.G., Shi, Y.M., Gao, F.P., 2020. Uplift soil resistance to a shallowly-buried pipeline in the sandy seabed under waves: poro-elastoplastic modeling. Appl. Ocean Res. 95, 102024.

Sassa, S., Sekiguchi, H., 1999. Wave-induced liquefaction of beds of sand in a centrifuge. Geotechnique 49 (5), 621–638.

Sassa, S., Sekiguchi, H., 2001. Analysis of wave-induced liquefaction of sand beds. Geotechnique 51 (2), 115–126.

Sassa, S., Takayama, T., Mizutani, M., Tsujio, D., 2006. Field observations of the build-up and dissipation of residual pore pressures in seabed sands under the passage of storm waves. J. Coast. Res. Spec. Iss. 39, 410–414.

Sawicki, A., Mierczyński, J., 2006. Developments in modeling liquefaction of granular soils caused by cyclic loads. Appl. Mech. Rev. 59 (2), 91–106.

Scholtès, L., Chareyre, B., Michallet, H., et al., 2015. Modeling wave-induced pore pressure and effective stress in a granular seabed. Continuum Mech. Therm. 27 (1–2), 305–323.

Seed, H.B., Lee, K.L., 1966. Liquefaction of saturated sands during cyclic loading. J. Soil Mech. Found. Div. ASCE 92 (SM6), 105–134.

Shi, Y.M., Gao, F.P., Wang, N., Yin, Z.Y., 2021. Coupled flow-seepage-elastoplastic modeling for competition mechanism between lateral instability and tunnel erosion of a submarine pipeline, 2021 J. Mar. Sci. Eng. 9 (8), 889.

Sumer, B.M., Fredsøe, J., Christensen, S., Lind, M.T., 1999. Sinking/floatation of pipelines and other objects in liquefied soil under waves. Coast Eng. J. 38, 53–90.

Sumer, B.M., 2014. Liquefaction Around Marine Structures. World Scientific Press, New Jersey.

Thomas, G.P., 1981. Wave-current interactions: an experimental and numerical study. Part 1. Linear waves. J. Fluid Mech. 110, 457–474.

Tsui, Y., Helfrich, S.C., 1983. Wave-induced pore pressures in submerged sand layer. J. Geotech. Eng. ASCE 109 (4), 603–618.

Vanneste, D., Troch, P., 2012. An improved calculation model for the wave-induced pore pressure distribution in a rubble-mound breakwater core rubble-mound breakwater core. Coast. Eng. 66, 8–23.

Whitham, G.B., 1962. Mass, momentum and energy flux in water waves. J. Fluid Mech. 12, 135–147.

Yamamoto, T., Koning, H.L., Sellmeijer, H., Hijum, E.V., 1978. On the response of a poro-elastic bed to water waves. J. Fluid Mech. 87, 193–206.

Ye, J., 2012. 3D liquefaction criteria for seabed considering the cohesion and friction of soil. Appl. Ocean Res. 37, 111–119.

Ye, J.H., Jeng, D.S., 2012. Response of porous seabed to nature loadings: waves and currents. J. Eng. Mech. 138 (6), 601–613.

Zen, K., Yamazaki, H., 1990. Mechanism of wave-induced liquefaction and densification in seabed. Soils Found. 31 (4), 161–104.

Zen, K., Yamazaki, H., 1991. Field observation and analysis of wave-induced liquefaction in seabed. Soils Found. 31 (4), 90–104.

Zhang, Y., Jeng, D.S., Gao, F.P., Zhang, J.S., 2013. An analytical solution for response of a porous seabed to combined wave and current loading. Ocean Eng. 57, 240–247.

Zhao, H.Y., Jeng, D.S., Liao, C.C., Zhu, J.F., 2017. Three-dimensional modeling of wave-induced residual seabed response around a mono-pile foundation. Coast. Eng. 128, 1–12.

Zhou, M.Z., Jeng, D.S., Qi, W.G., 2020. A new model for wave-induced instantaneous liquefaction in a non-cohesive seabed with dynamic permeability. Ocean Eng. 213, 107597.

Zhou, M.Z., Qi, W.G., Jeng, D.S., Gao, F.P., 2021a. A non-Darcy flow model for a non-cohesive seabed involving wave-induced instantaneous liquefaction. Ocean Eng. 239, 109807.

Zhou, M.Z., Liu, H., Jeng, D.S., Qi, W.G., Fang, Q., 2021b. Modelling the wave-induced instantaneous liquefaction in a non-cohesive seabed as a nonlinear complementarity problem. Comput. Geotech. 137, 104275.

Zou, Z.L., 2004. Water Wave Theories and Their Applications. Science China Press, Beijing.